Journal of Power Sources 180 (2008) 461–467

Contents lists available at ScienceDirect

Journal of Power Sources

journal homepage: www.elsevier.com/locate/jpowsour

An experimental study and model validation of a membrane humidifier for PEM fuel cell humidification control

Dongmei Chen [a], Wei Li [b,*], Huei Peng [a]

[a] Department of Mechanical Engineering, The University of Michigan, Ann Arbor, MI 48109, USA
[b] Department of Mechanical Engineering, University of Washington, Seattle, WA 98195-2600, USA

ARTICLE INFO

Article history:
Received 15 December 2007
Received in revised form 13 February 2008
Accepted 14 February 2008
Available online 29 February 2008

Keywords:
Polymer electrolyte membrane fuel cell
Humidification control
Membrane humidifier
Membrane vapor transfer coefficient
Non-minimum phase

ABSTRACT

This paper presents an experimental study and model validation of an external membrane humidifier for PEM fuel cell humidification control. Membrane humidification behavior was investigated with steady-state and dynamic tests. Steady-state test results show that the membrane vapor transfer rate increases significantly with water channel temperature, air channel temperature, and air flow rate. Water channel pressure has little effect on the vapor transfer rate and thus can be neglected in the system modeling. Dynamic test results reveal that the membrane humidifier has a non-minimum phase (NMP) behavior, which presents extra challenges for control system design. Based on the test data, a new water vapor transfer coefficient for Nafion membrane was obtained. This coefficient increases exponentially with the membrane temperature. The test results were also used to validate a thermodynamic model for membrane humidification. It is shown that the model prediction agrees well with the experimental results. The validated model provides an important tool for external humidifier design and fuel cell humidification control.

1. Introduction

Maintaining proper membrane humidity is one of the key requirements for the polymer electrolyte membrane (PEM) fuel cell to reach its optimum performance and to compete with the internal combustion engine as the future automotive power source [1]. Both membrane dehydration and flooding will cause poor fuel cell performance, as well as degraded fuel cell life [2–5]. Since water generation in a PEM fuel cell is a function of current demand, which is affected by the vehicle driving condition, a separate device is required to compensate for the humidity fluctuation of the PEM fuel cell systems.

Many PEM fuel cell humidification systems have been studied in the past. The most common ones are nozzle spray, gas bubbling, enthalpy wheel [6], and membrane humidification. The nozzle spray system involves atomizing coolant water that has left the power production section of the fuel cell and spraying the droplets uniformly onto a cloth or wire mesh for the reactant gases to go through. The method is simple; however, sensitive to temperature variation. If not preheated the amount of water absorbed by the inlet air will be affected by its temperature. As the cold air enters and reaches the operating temperature of the fuel cell stack, the relative humidity (RH) of the air will decrease, causing the fuel cell performance to vary. The gas bubbling method passes reactant gases through bottles of heated water. A considerable pressure drop across the gas bubbling humidifier is inevitable [7]. To compensate for the pressure drop, elevated inlet air pressure is required. Therefore, the gas bubbling technique is usually only suitable for small and low-pressure fuel cells. The enthalpy wheel method was recently developed, with a rotating ceramic wheel as the medium for both heat and humidity exchange. The inlet air humidification and heating is achieved using the hot and humid exhaust gas from the fuel cell itself. The humidity of the air is controlled by the rotational speed of the wheel, or if needed by controlling the opening of a bypass that determines how much of the exhaust gas is directed toward the enthalpy wheel. While it may reduce the concerns of added weight and parasitic loss, the enthalpy wheel method may cause cross-flows and is less desirable to automakers because of its complexity and potential maintenance cost.

Membrane humidifiers have been widely used for gas humidification and are under intensive study for PEM fuel cell applications [8]. The humidifier consists of a dry gas channel and a water or humid gas channel, separated by a water permeable membrane. While flowing, water vapor penetrates through the membrane from the water/humid gas channel to the dry gas channel due to the relative humidity gradient across the membrane. As a result, the inlet dry gas is humidified. The membrane humidifier can be designed to recycle the energy generated by the fuel cell without using a rotat-

* Corresponding author. Tel.: +1 206 543 5339; fax: +1 206 685 8047.
E-mail address: weiwli@u.washington.edu (W. Li).

0378-7753/$ – see front matter © 2008 Elsevier B.V. All rights reserved.
doi:10.1016/j.jpowsour.2008.02.055

ing part. There are no cross-flow concerns between the dry air and water channels. Furthermore, the membrane humidifier does not have the temperature and pressure drop associated with the nozzle spray and gas bubbling systems. Therefore, it is considered the best choice for PEM fuel cell humidity control [4].

A thermodynamic model of a membrane humidifier has recently been developed to capture the crucial dynamics of membrane humidification for PEM fuel cell humidity control [9]. Simulation results have shown that a cathode humidifier is necessary to maintain a high water content of the fuel cell membrane, whereas an anode humidifier is not needed. The performance of the humidifier is affected by the inlet air and water conditions, such as the flow rate, temperature and relative humidity. The thermodynamic model can be used for steady-state humidifier sizing. More importantly, it can be used to predict the transient behavior of the membrane humidifier for control system design.

In this paper, we present an experimental study of the membrane humidifier behavior and the validation of the thermodynamic humidification model for PEM fuel cell humidity control. Both steady-state and dynamic tests were conducted in controlled experiments. The membrane vapor transfer rate was characterized at various operating conditions including air flow rate, water channel temperature, air channel temperature, and water channel pressure. Based on the test results, a membrane vapor transfer coefficient was determined. With this coefficient, the predictions of the thermodynamic model were validated for both the steady-state and dynamic test results.

2. The membrane humidifier model

A schematic of the membrane humidifier in this study is shown in Fig. 1 [9]. The membrane is sandwiched between two channel plates with straight channels for water and air, respectively. The backing layers are used to protect the thin membrane. Fuel cell cooling water is used to humidify the dry inlet air. The dry inlet air flows into one of the channel plates and the fuel cell cooling water flows into the other. Heat and water vapor exchange across the membrane. Only one unit of the humidifier is shown in the figure. A number of such units can be stacked up depending on the humidity requirement of the fuel cell. The entire humidifier is insulated from the surrounding such that the heat and mass leaks are minimized.

Fig. 2 shows the definition of the control volumes for the thermodynamic model. Control Volume 1 contains the dry air to be humidified. Control Volume 2 contains the fuel cell cooling water used as the humidity source. For Control Volume 1, the mass flow

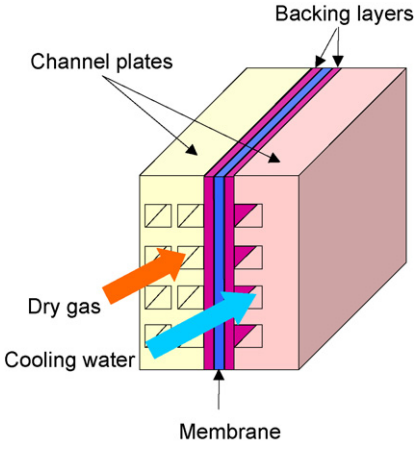

Fig. 1. Humidifier structure.

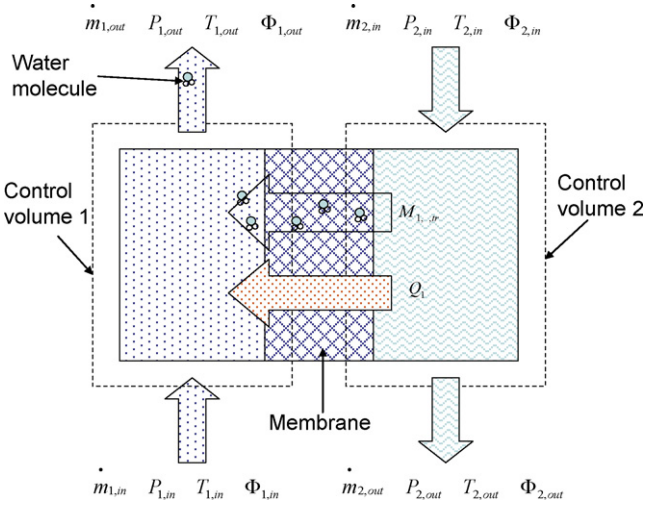

Fig. 2. Control volumes of a single humidifier unit.

rate, pressure, temperature, and relative humidity of the inlet air are denoted as $\dot{m}_{1,\text{in}}$, $P_{1,\text{in}}$, $T_{1,\text{in}}$, and $\Phi_{1,\text{in}}$, respectively. Those of the outlet air are denoted as $\dot{m}_{1,\text{out}}$, $P_{1,\text{out}}$, $T_{1,\text{out}}$, and $\Phi_{1,\text{out}}$. Similarly, for Control Volume 2, the mass flow rate, pressure, temperature, and RH of the cooling water are denoted as $\dot{m}_{2,\text{in}}$, $P_{2,\text{in}}$, $T_{2,\text{in}}$ and $\Phi_{2,\text{in}}$, respectively. Those of the outlet cooling water are denoted as $\dot{m}_{2,\text{out}}$, $P_{2,\text{out}}$, $T_{2,\text{out}}$ and $\Phi_{2,\text{out}}$. Between Control Volumes 1 and 2, the amounts of vapor and heat transfer are denoted as $m_{1,\text{v,tr}}$ and Q_1, respectively. The dry air and the cooling water are assumed to flow in either a parallel or a counter flow pattern.

The energy equation for Control Volume 1 can be expressed as [9]

$$\sum(\dot{m}_1 u_1 + m_1 \dot{u}_1) = \dot{Q}_1 + \sum(\dot{m}_{1,\text{in}} h_{1,\text{in}}) + (\dot{m}_{1,\text{v,tr}} h_{1,\text{v,tr}}) - \sum(\dot{m}_{1,\text{out}} h_{1,\text{out}}) \quad (1)$$

where

$$\dot{m}_1 = \dot{m}_{1,\text{in}} - \dot{m}_{1,\text{out}} \quad (2)$$

$$u_1 = \int C_{v\_1} \dot{T}_{1,\text{out}} \quad (3)$$

$$h_{1,\text{in}} = \int C_{p\_1,\text{in}} \dot{T}_{1,\text{in}} \quad (4)$$

$$h_{1,\text{out}} = \int C_{p\_1,\text{out}} \dot{T}_{1,\text{out}} \quad (5)$$

$$h_{1,\text{v,tr}} = \int C_{p\_v} \dot{T}_{\text{mem}} \quad (6)$$

C_{v_1} is the specific heat of gas with a constant volume, $C_{p\_1,\text{in}}$, $C_{p\_1,\text{out}}$ and C_{p_v} are the specific heat of the inlet, outlet and transferred gas with a constant pressure. T_{mem} represents the temperature of the membrane.

The energy equation for Control Volume 2 can be expressed in the same way, except that the heat and vapor transfer terms $\dot{Q}_1$ and $\dot{m}_{1,\text{v,tr}}$ should have negative signs in the right hand side of the equation. This is due to the model assumption that the heat and mass transfer is always from Control Volume 2 to Control Volume 1.

The heat transfer rate $\dot{Q}_1$ between the two control volumes can be obtained as [10]

$$\dot{Q}_1 = UA\Delta T_{2/1} \quad (7)$$

where U is the coefficient of heat transfer, A is the area of the membrane, and $\Delta T_{2/1}$ is the temperature difference between the two channels.

The membrane vapor transfer rate $\dot{m}_{1,v,tr}$ between the control volumes is calculated as [11,12]

$$\dot{m}_{1,v,tr} = D_w \frac{C_2 - C_1}{t_m} G_v A \tag{8}$$

where D_w is the membrane vapor transfer coefficient, G_v is the vapor molar mass, t_m is the thickness of the membrane, and C_1 and C_2 are the volumetric concentrations of the membrane matrix in contact with air and water, respectively. C_1 and C_2 can be calculated as

$$C_1 = \frac{\rho_{m,dry}}{M_{m,dry}} \lambda_1 \tag{9}$$

$$C_2 = \frac{\rho_{m,dry}}{M_{m,dry}} \lambda_2 \tag{10}$$

In the above equations $\rho_{m,dry}$ is the membrane dry density, $M_{m,dry}$ is the membrane dry equivalent weight, and λ_1 and λ_2 are the water contents per side chain of the membrane.

The water content at the air side λ_1 can be obtained as [11,12]

$$\lambda_1 = (0.043 + 17.81a_1 - 39.85a_1^2 + 36.0a_1^3) \tag{11}$$

where a_1 is defined as

$$a_1 = \frac{P_{1,v}}{P_{1,sat}} = \Phi_{1,out} \tag{12}$$

It is easy to recognize that a_1 in Eq. (12) is the relative humidity of the outlet air $\Phi_{1,out}$, $P_{1,v}$ is the vapor partial pressure of Control Volume 1, which can be obtained from the ideal gas law. $P_{1,sat}$ is the saturation pressure of Control Volume 1, which can be obtained as [13]

$$\log_{10}(P_{1,sat}) = -1.69 \cdot 10^{-10} T_{1,out}^4 + 3.85 \cdot 10^{-7} T_{1,out}^3 - 3.39 \cdot 10^{-4} T_{1,out}^2 + 0.143 T_{1,out} - 20.92 \tag{13}$$

It should be noted that Eq. (11) was experimentally obtained for Nafion membrane N117, which is the type of membrane used in this study. It is by no means universally applicable to all fuel cell membranes. For other types of membranes, this relationship needs to be determined before it can be used in the membrane humidification model.

According to Schroeder's paradox [14], the water content at the water channel side λ_2 could be any value between 14 and 22 for a Nafion membrane. It is 14 when the membrane is in equilibrium with saturated vapor and 22 when the membrane is in equilibrium with liquid water. In our study, the membrane water content is in between the above two conditions. Therefore, a suitable water content value λ_2 will be determined based on experimental data.

The vapor transfer coefficient D_w in Eq. (8) can be determined using the following equation [11]

$$D_w = D_\lambda e^{E_o(1/303 - 1/T)} \tag{14}$$

where T is the membrane temperature, E_o is associated with the water molecule activation energy, and D_λ has a piecewise-linear form [11,12]

$$D_\lambda = \begin{cases} 10^{-1} & \lambda_m < 2 \\ 10^{-6}(1 + 2(\lambda_m - 2)) & 2 \le \lambda_m \le 3 \\ 10^{-6}(3 - 1.67(\lambda_m - 3)) & 3 < \lambda_m < 4.5 \\ 1.25 \times 10^{-6} & \lambda_m \ge 4.5 \end{cases} \tag{15}$$

In the above equation λ_m is the membrane water content and can be defined as

$$\lambda_m = 0.043 + 17.81a_m - 39.85a_m^2 + 36.0a_m^3 \tag{16}$$

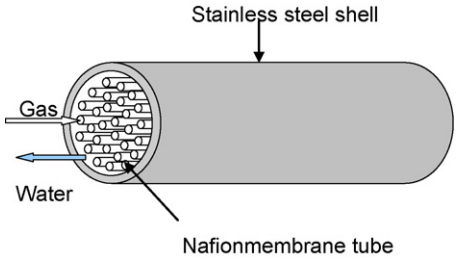

Fig. 3. Perma Pure water to gas humidifier.

Table 1
Perma Pure humidifier specification

Nafion tube ID	1.32 mm
Nafion tube OD	1.6 mm
Nafion tube length	610 mm
Number of tubes	60
Stainless steel shell ID	25 mm
Stainless steel length	610 mm

where a_m is the membrane RH and can be determined as

$$a_m = \frac{\Phi_1 + \Phi_2}{2} \tag{17}$$

Φ_1 and Φ_2 are the relative humidity of Control Volume 1 and Control Volume 2.

The water activation energy E_o in Eq. (14) was chosen to be 2416 in the Spring model [11]. This value was as determined by Yeo and Eisenberg [15] for a steady-state equilibrium condition within a local membrane area. In our study, however, the membrane humidifier operates in a dynamic condition. There could be other factors involved in the mass transfer process, such as the variation along the channel and the transport resistance in the boundary layer. Therefore, the value of E_o will also be determined based on the experimental data in this study.

3. Experimental

A Nafion membrane humidifier, Perma Pure®[1] model PH-60T-24SS, was used in this study to examine the membrane humidification behavior and to verify the thermodynamic model. The humidifier had 60 Nafion membrane tubes installed in a stainless steel shell as shown in Fig. 3. The dry gas flowed inside the membrane tubes, while the water counter-flowed between the membrane tubes and the stainless steel shell. The humidifier dimensions are listed in Table 1. The thermodynamic model developed based on the geometry shown in Fig. 1 can be applied to the tubular membrane humidifier by substituting the corresponding parameters into the model. For instance, the flat membrane area is replaced by the cylindrical tube area. The heat transfer coefficient is the same since both structures have the same hydraulic diameter.

Fig. 4 shows a schematic of the experimental setup. It has two paths, one for air and the other for water. In the air path, the compressed air first went through an air filter to remove any contamination. It was then regulated with a flow controller (OMEGA Engineering, FMA-2609A-NIST) before going through a heating chamber (OMEGA Engineering, AHPF-121). The air subsequently went through the Nafion membrane tubes to be humidified and in the end exited to the atmosphere. In the water path, distilled water from a water tank was fed into the gap between the membrane tubes and the stainless steel shell. A heating pad wrapping around the outside of the stainless steel shell was used to control the water

[1] Perma Pure® is a registered trademark of Perma Pure, Inc.

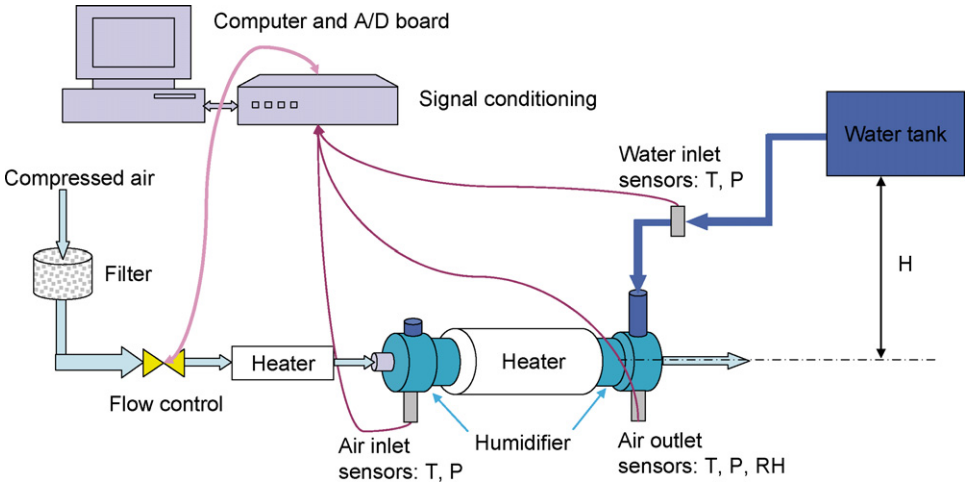

Fig. 4. A schematic of the experimental setup *T*: temperature, *P*: pressure, RH: relative humidity.

temperature. The water channel pressure was adjusted by changing the water tank location, Dimension H, as shown in the figure. Two pressure transducers (OMEGA Engineering, PX41T0-100G5V) and two thermocouples (OMEGA Engineering, TMTSS-062G-6 and SA1-T) were installed at the inlet and the outlet of the humidifier to measure the corresponding pressures and temperatures. An integrated humidity and temperature sensor (VAISALA, HMP238) was connected to the outlet of the humidifier to measure the relative humidity and temperature of the outlet air. A computer data acquisition system (NATIONAL INSTRUMENTS, PCI-6024E and SC-2345) were used to record all the sensor readings, as well as to control the air flow rate through the OMEGA flow controller.

Both steady-state and dynamic tests were conducted in the study. The steady-state tests were used to examine the effects of air flow rate, inlet air temperature, water channel temperature, and water channel pressure. Although the relative humidity of the outlet air was directly measured, the response variable of the steady-state test was chosen to be the membrane vapor transfer rate. This is because that the relative humidity is a function of both the vapor transfer rate and the air temperature. In the steady-state test, we are more interested in the mass transfer rate of water molecules as affected by the humidifier conditions. Therefore, we compare the membrane vapor transfer rate instead of the air outlet relative humidity.

The experimental conditions for the steady-state tests are listed in Table 2. To determine the effects of air flow rate, the air temperatures was set at 24 and 27 °C, the water temperature at 19 °C, the water pressure at 0 cm H_2O, and the air flow rate varied from 0 to 50 slm. To determine the effects of the inlet air temperature, the water flow temperature was set at 17 °C, the air flow rate at 50 slm, the water pressure at 0 cm H_2O, and the inlet air temperature varied from 20 to 40 °C. To determine the effects of the water channel temperature, the air temperature was set at 22 °C, the air flow rate at 50 slm, the water channel pressure at 0 cm H_2O, and the water channel temperature varied from 10 to 40 °C. Finally, to determine the effects of the water channel pressure, the air temperature was set at 22 °C, the air flow rate at 50 slm, the water temperature at 17 °C, and the water channel pressure varied from 0 to 71 cm and 135 cm H_2O.

The dynamic test was conducted with a varying inlet air flow rate. In the automotive fuel cell application, while other variables may be slow changing, the air flow rate can change rapidly as current demand from the fuel cell changes. The dynamic response of the humidifier is thus very important to the performance of fuel cells, especially for the automotive application. In this study, the dynamic response of the membrane humidification was examined by setting the air temperature at the ambient temperature (24–27 °C), water temperature at 19 °C, water pressure at 0 cm H_2O, and varying the air flow rate from 10 to 40 slm. Relative humidity is used as the response variable to compare with the model predictions.

4. Results and discussion

4.1. Steady-state results

In the experimental study the following signals were recorded over time: the inlet air temperature $T_{1,in}$, the inlet air pressure $P_{1,in}$, the inlet air flow rate $\dot{m}_{1,in}$, the outlet air RH $\Phi_{1,out}$, the outlet air temperature $T_{1,out}$, the outlet air pressure $P_{1,out}$, and the water temperature $T_{2,out}$. Based on the recorded values, the membrane vapor transfer rate was computed as [10]

$$\dot{m}_{1,v,tr} = \rho_a \omega_{a,out} \dot{m}_{1,in} \tag{18}$$

where

$$\omega_{a,out} = \frac{G_v P_{1,sat} \Phi_{1,out}}{G_a P_{1,v}} \tag{19}$$

ρ_a is the air density (1.2 kg m^{-3}), G_v is the vapor molar mass (0.01802 kg mol^{-1}), G_a is air molar mass (0.029 kg mol^{-1}), $P_{1,sat}$ is the vapor saturation pressure that can be calculated using Eq. (13), and $P_{1,v}$ is the partial vapor pressure of the air channel and can be calculated using the ideal gas law.

Table 2
Experimental conditions for the steady-state test

Studied effect	Air temperature (°C)	Water temperature (°C)	Water pressure (cm H_2O)	Air flow rate (slm)
Air flow rate	24, 27	19	0	0–50
Air temperature	20–40	17	0	50
Water temperature	22	10–40	0	50
Water pressure	22	17	0, 71, 135	50

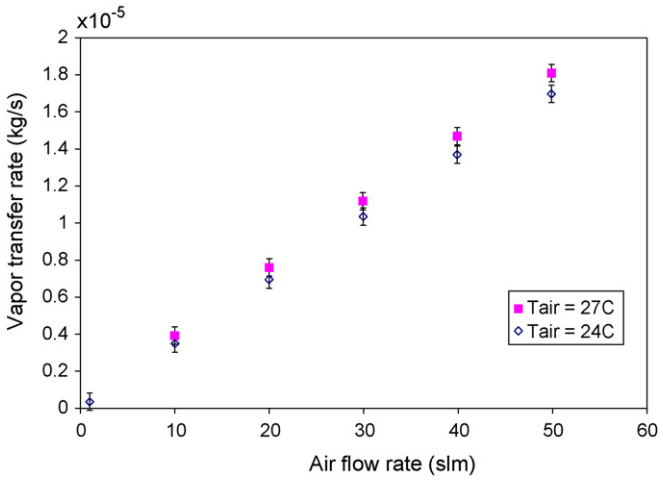

Fig. 5. Air flow rate effect on membrane vapor transfer rate.

Fig. 5 shows the steady-state test results of air flow rate effects. It can be seen that the membrane vapor transfer rate is proportional to the air flow rate. The faster the air flow is, the higher the vapor transfer rate will be. When the air moves faster through the channel, there is a less chance for it to get fully humidified; therefore, the water vapor gradient across the membrane remains high at a high air flow rate. As a result, more water molecules will pass across the membrane from the water side to the air side at any given time.

The test result of the inlet air temperature effect is shown in Fig. 6. It can be seen that the water vapor transfer rate increases almost linearly with the inlet air temperature. The reason is two-fold. First, an increasing inlet air temperature will cause the membrane temperature to increase. It has been found that the higher the membrane temperature, the higher the membrane vapor transfer coefficient [11]. Thus, more vapor will pass through the membrane at a higher temperature. Second, an increasing inlet air temperature will increase the air channel temperature, which according to Eq. (13) will in turn increase the vapor saturation pressure of the air channel. From Eq. (12), the higher the vapor saturation pressure, the lower the relative humidity in the air channel. The water concentration C_1 in Eq. (8) is a monotonic function of the air channel relative humidity. As a result, the water concentration gradient across the membrane becomes larger and more vapor molecules will pass through the membrane.

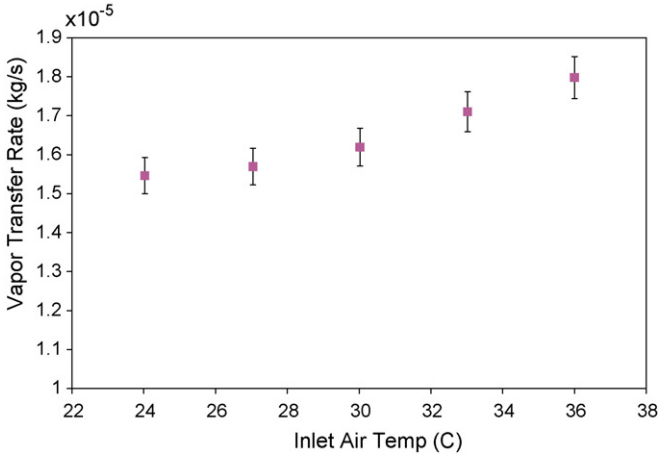

Fig. 6. Inlet air temperature effect on membrane vapor transfer rate.

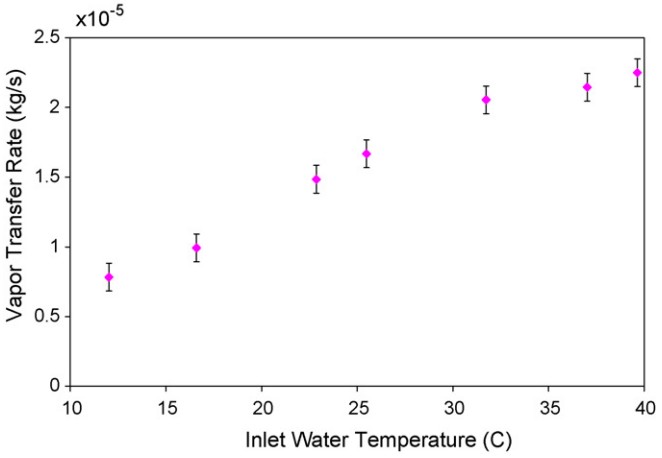

Fig. 7. Water channel temperature effect on membrane vapor transfer rate.

In addition to the inlet air temperature, the water channel temperature also affects the membrane vapor transfer rate. The test result of a varying water temperature is shown in Fig. 7. As can be seen, the membrane vapor transfer rate increases more significantly with the water temperature as compared to the air temperature. The vapor transfer rate increased by about 50% when the water temperature increased from 22 to 36 °C, while it only increased by 20% when the inlet air temperature had the same increase. This is due to the fact that the heat capacity of water is higher than that of air with the same temperature difference. As a result, the membrane is heated faster by water than by air.

The effect of water channel pressure is shown in Fig. 8. Three water channel pressures were tested. They were 0, 71, and 135 cm H_2O, corresponding to 0, 1 and 2 psi. It can be seen that the membrane vapor transfer rate increased only slightly over the range of the pressure change. This increase may not be statistically significant, as can be seen from the figure that the measurement error is almost comparable with the vapor transfer rate increase. Therefore, the effect of water channel pressure is neglected in this study.

4.2. Dynamic results

The dynamic test results of the air flow rate effects are shown in Fig. 9. It can be seen that the relative humidity of the outlet air increases as the inlet air flow rate steps down from 40 to 10 slm. The amount of this RH increase, however, is not the same at each

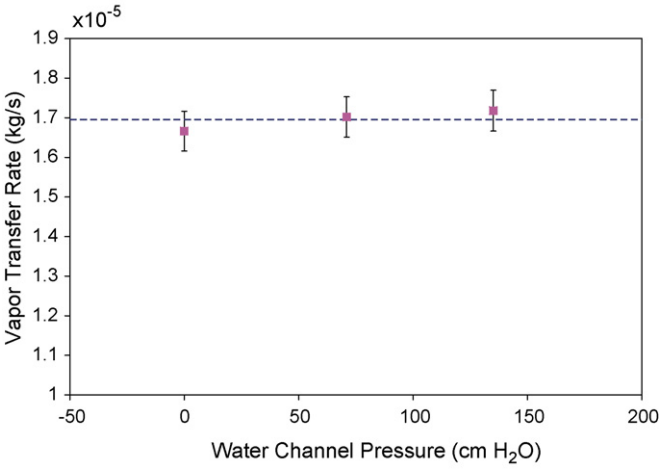

Fig. 8. Water channel pressure effect on membrane vapor transfer rate.

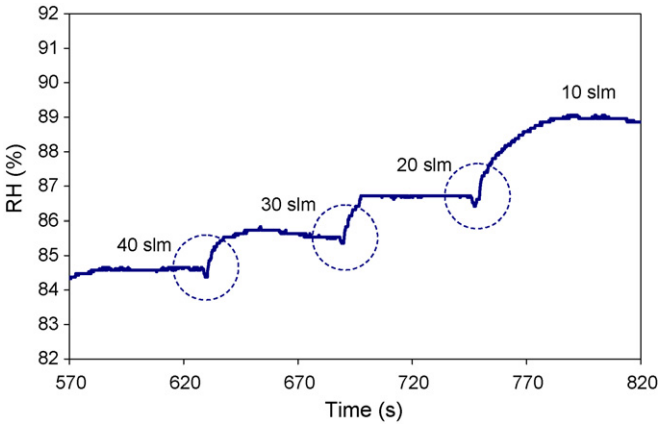

Fig. 9. Dynamic RH response as a function of varying air flow rate.

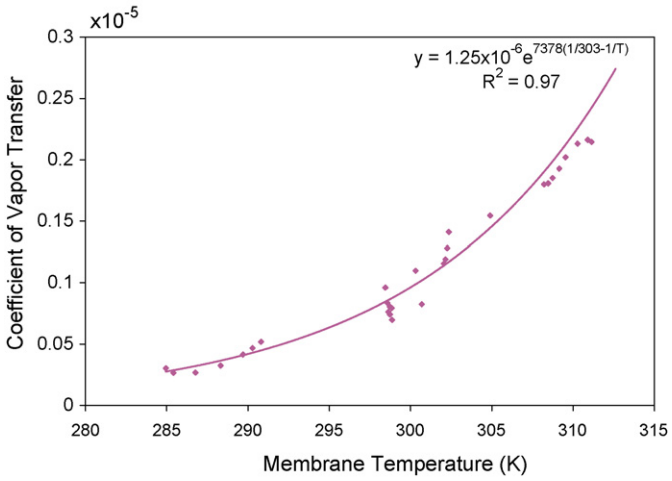

Fig. 10. Membrane vapor transfer coefficient as a function of temperature.

step-down. For example, when the inlet air flow rate reduced from 40 to 30 slm the RH increased by about 1%. When the flow rate reduced from 20 to 10 slm the RH increased by about 3%. Related to this difference is the response time difference at different air flow rates. It takes longer for the RH to reach the steady-state values when the air flow rate is lower.

Another important phenomenon observed in Fig. 9 is the initial reverse response of the relative humidity. When the air flow rate is changed from one level to another, the RH response does not immediately follow the steady-state trend. Instead, it goes toward the opposite direction first and then returns to the normal trend. In controls theory, this phenomenon is referred to as the non-minimum phase (NMP) behavior. It is often caused by the response time mismatch of two or more dynamic processes that involved in a system [16]. For the membrane humidification system in this study, the NMP behavior is caused by the lag of vapor transfer rate in Control Volume 1 comparing to the heat transfer rate between the two control volumes [17]. A non-minimum phase system presents a significant challenge for control design. To deal with this kind of systems, a predictive system model is usually required.

4.3. Model validation

The membrane humidifier model is validated both for the water vapor transfer rate and the non-minimum-phase behavior. The fundamental parameter in membrane humidification is the vapor transfer coefficient, which determines how fast the water molecules transfer through a membrane under certain conditions. The water vapor transfer coefficient for Nafion membrane has been determined in a series of well-known studies by Zawodzinski et al. [18–20] and widely used in fuel cell models. However, in previous studies the membrane was sandwiched between two gas chambers. Their test was conducted under steady-state equilibrium conditions. In our research the membrane was in contact with liquid water and exposed to a dynamic flow field. Our focus is to develop a lumped model that can be used for automatic control purposes. Therefore, the membrane vapor transfer rate in Eq. (8) used in this research is different from the Springer model. The parameters used to determine the membrane vapor transfer rate including λ_2 and E_o need to be estimated based on the experimental data in this research.

Fig. 10 shows the experimental data and a fitted empirical model of the membrane vapor transfer coefficient. The parameters λ_2 and E_o were determined to be 15.6 and 7378, respectively. The fact that λ_2 is 15.6 indicates that the membrane is under a transitional condition between being fully saturated with vapor and liquid water. It is interesting that E_o takes on a much higher value than the Yeo and Eisenberg water activation energy [15] that was use in the Springer model. This may be due to the fact that Yeo and Eisenberg used the data at low membrane RH (0–50%) in their experiment to obtain the activation energy and the water was mostly in the vapor phase. The Yeo and Eisenberg study also showed that the activation energy would have been higher if they used the data with a higher membrane RH (>50%). In this study the membrane was sandwiched between water and vapor and the membrane had high RH (>80%). In addition, the water was mostly in the liquid phase. As such extra energy may be required to vaporize the water before the vapor was driven through the membrane.

Substituting the values of the above two parameters, Eq. (8) becomes

$$\dot{m}_{1,v,tr} = D_w(15.6 - \lambda_1)\frac{\rho_{m,dry}}{M_{m,dry}}\frac{G_V A}{t_m} \quad (20)$$

and Eq. (14) becomes

$$D_w = D_\lambda e^{7378(1/303-1/T)} \quad (21)$$

After the parameters were determined, new tests were conducted to validate the model. These new tests were conducted at air flow rate and water temperature conditions other than those used to determine the model parameters. Both steady-state and dynamic predictions were validated. The result of the steady-state validation is shown in Fig. 11. It compares the model-predicted vapor transfer rates with those obtained from the new experimental data. The

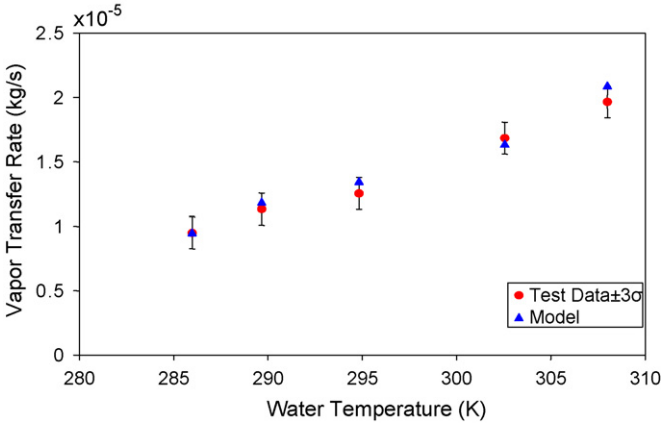

Fig. 11. Steady-state validation results. Experiments conducted at 50 slm air flow rate, room temperature for the inlet air, and water temperature varying from 14 to 35 °C.

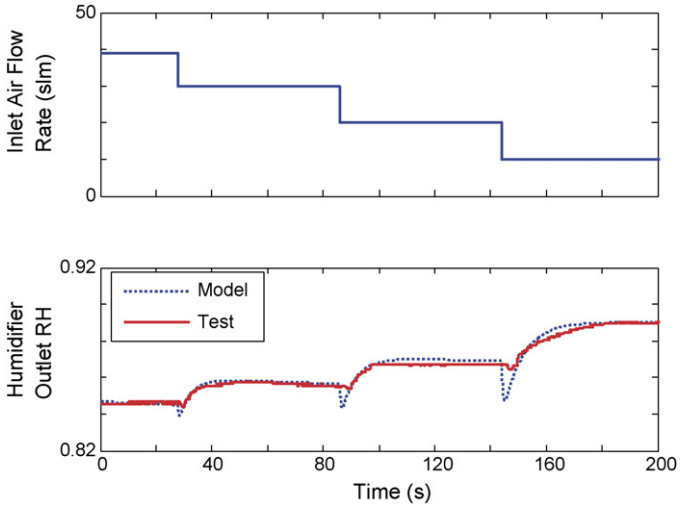

Fig. 12. Dynamic validation results. Air flow rate: 40–10 slm with 10 slm step-downs; air inlet temperature: 26 °C; water temperature: 19 °C.

results show that the model prediction is in good agreement with the new test data over a range of temperatures. Tests were also conducted to verify the dynamic behavior revealed in the simulation results. The comparison between the model predictions and the experimental results under the dynamic condition is shown in Fig. 12. In the dynamic test the air flow rate decreased from 40 to 10 slm with a step of 10 slm, the air temperature was 26 °C and the water temperature was 19 °C. The model predictions match the test results closely, for both the NMP behavior and the step changes of RH. Nevertheless, the figure shows that the model predicts a stronger NMP characteristic than the test results. This is due to the slow dynamics of the RH sensor. According to the manufacturer specification, the Vaisala HMP238 sensor has a 15 s response delay. This delay causes the sensor to act effectively as a low pass filter, which will attenuate the non-minimum phase behavior of the RH signals.

5. Conclusions

This paper presented an experimental study of a membrane humidifier and the validation of a thermodynamic humidification model for PEM fuel cell humidity control. Both steady-state and dynamic tests were conducted in controlled experiments. The steady-state test results show that the membrane vapor transfer rate increases with the temperatures of the inlet air and water and decreases with the air flow rate. The water channel pressure has little effect on the membrane vapor transfer rate and thus can be neglected. A non-minimum phase behavior is observed in the dynamic tests. It is caused by the response time mismatch in the membrane humidification system. Based on the test results a new vapor transfer coefficient of Nafion membrane is obtained for dry air humidification by liquid water. This vapor transfer coefficient has a characteristic of exponentially increase with temperature. The thermodynamic humidifier model is validated using both the steady-state and dynamic test data. The validated model provides an important tool for external humidifier design and fuel cell humidification control.

References

[1] J.T. Pukrushpan, H. Peng, A.G. Stefanopoulou, Simulation and analysis of transient fuel cell system performance based on a dynamic reactant flow model, in: Proceeding of 2002 ASME International Mechanical Engineering Congress & Exposition, New Orleans, Louisiana, Nov. 17–22, 2002.
[2] D. Chu, R. Jiang, C. Walker, Analysis of PEM fuel cell stacks using an empirical current-voltage equation, Journal of Applied Electrochemistry 30 (2000) 365–370.
[3] P.A. Chuang, A. Turhan, A.K. Heller, J.S. Brenizer, T.A. Trabold, M.M. Mench, The nature of flooding and drying in polymer electrolyte fuel cells, in: Proceedings of FUELCELL2005 Third International Conference on Fuel Cell Science, Engineering and Technology, Ypsilanti, Michigan, USA, May 23–25, 2005.
[4] P. Sridhar, R. Perumal, N. Rajalakshmi, M. Raja, K.S. Dhathathreyan, Humidification studies on polymer electrolyte membrane fuel cell, Journal of Power Sources 101 (2001) 72–78.
[5] M. Ceraolo, C. Miulli, A. Pozio, Modelling static and dynamic behavior of proton exchange membrane fuel cells on the basis of electro-chemical description, Journal of Power Sources 113 (2003) 131–144.
[6] R.A. Dubose, Enthalpy Wheel Humidifiers, Presentation from 2002 Fuel Cell Seminar.
[7] D. Chu, R.Z. Jiang, Performance of polymer electrolyte membrane fuel cell (PEMFC) stacks part I. Evaluation and simulation of an air-breathing PEMFC stack, Journal of Power Sources 83 (1999) 128–133.
[8] D. Picot, R. Metkemeijer, J.J. Bezian, L. Rouveyre, Impact of the water symmetry factor on humidification and cooling strategies for PEM fuel cell stacks, Journal of Power Sources 75 (1998) 251–260.
[9] D. Chen, H. Peng, A thermodynamic model of membrane humidifiers for PEM fuel cell humidification control, Journal of Dynamic Systems, Measurement, and Control 127 (3) (2005) 424–432.
[10] F.P. Incropera, D.P. DeWitt, Introduction to Heat Transfer, third ed., John Wiley & Sons, Inc., 1996.
[11] T.E. Springer, T.A. Zawodzinski, S. Gottesfeld, Polymer electrolyte fuel cell model, Journal of Electrochemical Society 138 (8) (1991) 2334–2342.
[12] T.V. Nguyen, R.E. White, A. Water, Heat management-membrane fuel cells, Journal of Electrochemical Society 140 (8) (1993) 2178–2186.
[13] R.E. Sonntag, C. Borgnakke, G.J. Van Wylen, Fundamentals of Thermodynamics, fifth ed., John Wiley & Sons, Inc., 1998.
[14] A.Z. Weber, J. Newman, Transport in polymer-electrolyte membranes I. Physical model, Journal of The Electrochemical Society 150 (7) (2003) 1008–1015.
[15] S.C. Yeo, A. Eisenberg, Physical properties and supermolecular structure of perfluourinated ino-containing(Nafion) polymers, Journal of Applied Polymer Science 21 (1977) 875–898.
[16] D.K. Miu, B. Yang, On transfer function zeros of general collocated control systems with mechanical flexibilities, ASME Journal of Dynamic System, Measurement and Control 116 (1994) 151–154.
[17] D. Chen, H. Peng, Non-minimum phase behavior of PEM fuel cell membrane humidification systems, ASME Journal of Dynamic System, Measurement and Control, in press.
[18] T.A. Zawodzinski, M. Neeman, L.O. Sillerud, S. Gottesfeld, Determination of water diffusion coefficients in perfluorosulfonate ionomeric membranes, Journal of Physical Chemistry 95 (1991) 6040–6044.
[19] T.A. Zawodzinski, C. Derouin, S. Radzinski, R.J. Sherman, V.T. Smith, T.E. Springer, S. Gottesfeld, Water uptake by and transport through Nafion® 117 membranes, Journal of Electrochemical Society 140 (4) (1993) 1041–1047.
[20] T.A. Zawodzinski, T.E. Springer, J. Davey, R. Jestel, C. Lopez, J. Valerio, S. Gottesfeld, A comparative study of water uptake by and transport through ionomeric fuel cell membranes, Journal of Electrochemical Society 140 (7) (1993) 1981–1985.